CHAPTER 6

Aircraft Engine Inlets and Nozzles

Source: Reproduced with permission from Rolls-Royce plc

6.1 Introduction

In this chapter, we study the aerothermodynamics of aircraft engine inlets and nozzles. These two components in an aircraft engine represent "duct" flows with internal losses and hence we propose to study them in a single chapter. Despite these similarities, the inlet flowfield bears no resemblance to the exhaust flowfield. The presence of adverse pressure gradient in an inlet diffuser leads to a stalling boundary layer behavior, whereas the favorable pressure gradient in a nozzle promotes attached boundary layer flows. Another dissimilarity between these two components is in the cooling requirements of an advanced exhaust system as compared with the inlets, which remain uncooled until well into the hypersonic flight Mach numbers.

The system requirements of an aircraft intake primarily depend on the aircraft *mission specification.* In general, an aircraft intake system has to be designed to many of the following qualities, namely

1. light weight and low cost to manufacture
2. provide the engine with adequate mass flow rate at a proper Mach number at the engine face throughout the flight envelope
3. provide *spatially smooth* flow into the engine compressor, that is, low *steady-state distortion* throughout the flight envelope
4. provide *temporally smooth* flow into the engine compressor, that is, low *dynamic distortion* throughout the flight envelope

Aircraft Propulsion, Second Edition. Saeed Farokhi.

Companion Website: www.wiley.com/go/farokhi

5. integrate well with the engine nacelle and/or fuselage, that is, *low installation drag*
6. provide acoustic absorption of fan/engine noise, that is, *quiet engine*
7. provide a particle separator for an engine in a vertical lift aircraft, that is, foreign object damage (FOD) *control*
8. provide low radar signature, that is, *low observables* for stealth requirement
9. provide favorable *"ilities,"* for example, accessibility, inspectability, reliability, maintainability, repairability
10. allow for engine *thrust growth*.

By a close inspection of the above "wish" list, we note several conflicting drivers that appear in the air inlet system design. Therefore, a team of engineers is tasked with seeking an "optimum compromise" for the design. The presence of conflicting requirements and seeking an optimal solution are invariably present in any commercial product development.

Our one-dimensional cycle analysis treated an aircraft engine component as a "black box," that is, the block approach. The "block" approach linked the exit condition of a component to its inlet condition via an efficiency parameter. For example, an exit total pressure of an inlet was linked to the inlet total pressure via the inlet adiabatic efficiency parameter η_d or the total pressure recovery parameter π_d. In turn, we treated the component efficiencies as an input to our cycle analysis. Now, we propose to look inside the black box and identify design features that affect the component efficiencies. Inevitably, we will need to examine the true multidimensional aspect of the flowfield in aircraft engine components.

6.2 The Flight Mach Number and Its Impact on Inlet Duct Geometry

It is customary to divide the inlet flowfield into subsonic and supersonic flow regimes. The flow in the subsonic portion of an inlet is dominated by its boundary layer behavior, whereas the supersonic portion of an inlet is dominated by the appearance of shocks and their interaction with the boundary layer on the compression ramps and the nacelle or fuselage. Hence, the emphasis is different in the two flows. In this section, we will examine the geometrical requirements for subsonic and supersonic diffusers.

From one-dimensional compressible flow studies in aerodynamics (Anderson, 2005) we learned that

$$\frac{dA}{A} = (M_\infty^2 - 1)\frac{dV}{V} \tag{6.1}$$

Hence for a subsonic duct flow, where $M_\infty < 1$, the flow deceleration, that is, $dV < 0$, requires an area increase, that is, $dA > 0$, in the duct. Therefore, a cross-sectional area increase in a duct causes a subsonic flow to decelerate. On the contrary, a supersonic deceleration requires a flow area shrinkage with a turning point occurring at $M = 1$, that is, the sonic point. This suggests a converging flow in the supersonic regime to achieve a sonic condition followed by a diverging duct to decelerate the flow to the desired subsonic speeds for a supersonic diffuser. An opposite behavior is observed in accelerating flows, such as those in nozzles. A subsonic flow is accelerated through a converging duct, that

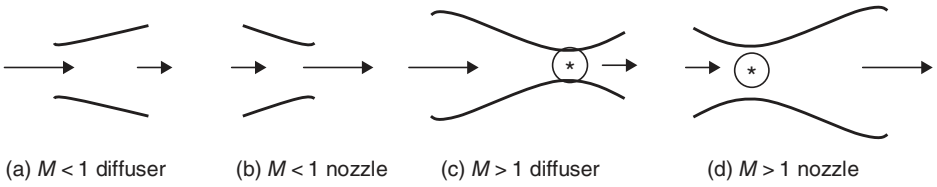

■ **FIGURE 6.1**
Geometric requirements for inlets and nozzles (* represents the sonic throat)

is, $dA < 0$, and a supersonic acceleration is achieved in a diverging duct, that is, $dA > 0$. Again, a supersonic nozzle needs to have a sonic "throat" before the diverging area begins for a supersonic acceleration. A schematic drawing of various duct geometries and flow regimes is shown in Figure 6.1.

6.3 Diffusers

Now, let us introduce some preliminary nomenclature in a subsonic diffuser. A more detailed geometry of a subsonic diffusing flow is shown in Figure 6.2, where x is the primary flow direction and y is the lateral or transverse flow direction. The symbols W and R stand for the width (in the diverging direction) of a rectangular and the radius of a conical diffuser, respectively. The axial diffuser length is called N and the diffuser wall length is depicted as L, in Figure 6.2. We also note that the diffuser wall inclination or divergence angle is shown as ϕ_w.

The thermodynamic states of a diffuser flow are shown in Figure 6.2 as well. Note the static pressure rise ($p_2 > p_1$), which is accompanied by a static temperature rise in the diffuser ($T_2 > T_1$). Also, we note a large inlet kinetic energy is shown in Figure 6.2, ($V_1^2/2c_p$), which diminishes to a small kinetic energy at the exit ($V_2^2/2c_p$). The flow stagnation enthalpy remains constant in an adiabatic diffuser, which is shown in Figure 6.2 as a constant total temperature process. Finally, we note that the total pressure at the exit of diffuser is lower than the inlet, which is the basis of an entropy rise Δs.

Now, we are ready to introduce a new performance parameter in a diffuser. This new parameter accounts for the *static* pressure rise in a diffuser, which essentially characterizes the conversion of fluid kinetic energy into the fluid static pressure. Note that in a compressible flow, the kinetic energy converts into static pressure rise as well as the internal energy of the fluid, unlike an incompressible fluid where kinetic energy is

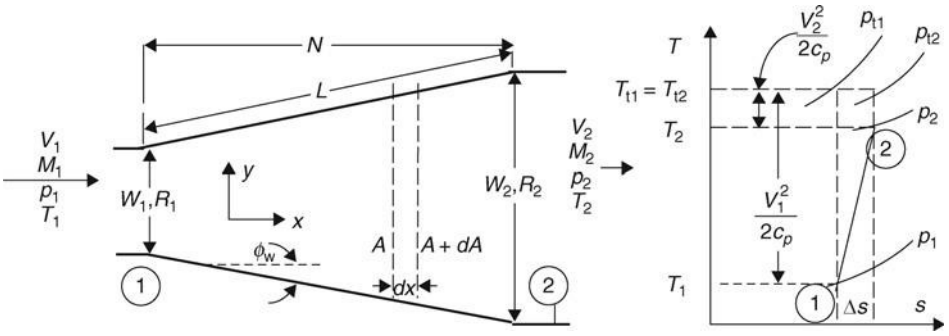

■ **FIGURE 6.2**
Definition sketch for a subsonic diffuser and a $T - s$ diagram depicting the static and stagnation states in a diffuser

converted to static pressure only. The nondimensional pressure rise parameter in a diffuser is called the static pressure recovery coefficient C_{PR} and is defined as

$$C_{PR} \equiv \frac{p_2 - p_1}{\bar{q}_1} = \frac{\Delta p}{\rho_1 \bar{V}_1^2/2} \tag{6.2}$$

The "bar" over q_1 in the denominator represents the mass-averaged velocity to be used in the dynamic pressure calculation. This reminds us that all internal flows contain boundary layers, which make the flow nonuniform (at least within the boundary layer). We will study this new parameter and other figures-of-merit in various diffuser environments. First, let us look at an *ideal* diffuser, where the fluid is both incompressible and inviscid.

6.4 An Ideal Diffuser

Applying the Bernoulli equation between stations 1 and 2 of a diffuser for an inviscid fluid, and using the continuity equation for a one-dimensional flow, we can relate the (ideal) diffuser performance $C_{PR,ideal}$ to the diffuser area ratio A_2/A_1 as follows:

$$C_{PR_{ideal}} = \frac{q_1 - q_2}{q_1} = 1 - \left(\frac{A_1}{A_2}\right)^2 = 1 - \frac{1}{AR^2} \tag{6.3}$$

where the AR depicts the diffuser exit-to-inlet area ratio. This statement shows that for a very large area ratio diffuser, the ideal static pressure recovery will approach 1. We expected this result, which states that the inlet dynamic pressure is entirely converted into static pressure rise in a duct if the exit area is infinitely large. Let us plot the ideal static pressure recovery coefficient C_{PR} versus the diffuser area ratio (Figure 6.3).

We note from the ideal diffuser pressure recovery Equation 6.3 that the shape of the cross section of the diffuser does not enter the problem, that is,

$$C_{PR_{ideal}} \neq f(\text{geometry})_{\text{crosssection}} \tag{6.4}$$

This is a consequence of our oversimplified picture of a diffusing flow in a single direction, which ignores viscosity of the fluid and thus boundary layer formation. Consequently, a

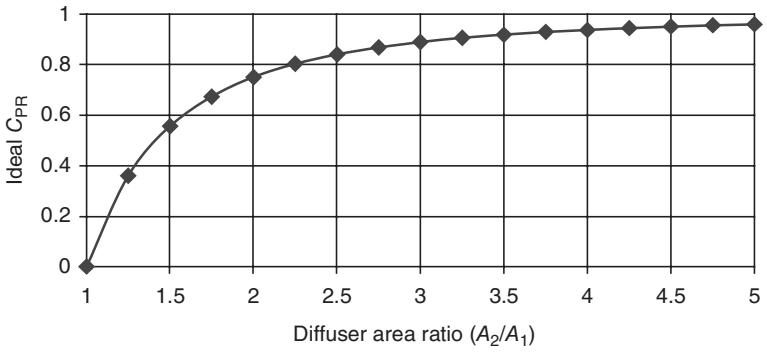

■ **FIGURE 6.3**
An ideal diffuser pressure recovery as a function of diffuser area ratio

major driver in diffuser performance, namely the cross-sectional shape and the shape of the diffuser centerline influencing the wall boundary layer flow, is ignored in the *ideal* flow analysis. We also note that a high static pressure recovery requires a large diffuser area ratio. We will return to this parameter, that is, the area ratio, later in this chapter.

6.5 Real Diffusers and Their Stall Characteristics

We recognize that in a real flow environment, boundary layers are formed, and have a tendency to separate when exposed to a rising static pressure, known as an adverse (streamwise) pressure gradient. Therefore, we expect the behavior of a diffuser to be driven by the viscous region near its walls, that is, the state of the boundary layer as in attached, separated, or transitory (unsteady). Consequently, the performance of a real diffuser should strongly depend on its inlet boundary layer condition. In addition, the geometry of the cross-section as well as the centerline curvature of a diffuser both influence the cross-flow tendency in the boundary layer and hence affect the three-dimensional separation characteristics of the diffuser. The formation of a skewed boundary layer is in direct response to a transverse (or lateral) pressure gradient in a diffuser duct. Therefore, we expect the geometry of the diffuser in both the streamwise area variation and the cross-sectional shape (and its streamwise variation), to be of great importance in the performance of a diffuser. The three basic geometries of interest are (Figure 6.4)

(a) two-dimensional rectangular
(b) axisymmetric, that is, conical
(c) annular.

Another feature of a real diffuser is the geometrical shape of its centerline. Often the engine face is hidden from an observer looking through the inlet. The feature of a hidden engine face offers the potential of masking the radar reflections off the engine face, which is advantageous in a stealth aircraft. In addition, fighter aircraft are often designed with their engine(s) inside the fuselage to leave the wings free to carry external weapons. The so-called "buried" engine design of such aircraft requires an S-shaped subsonic diffuser duct to channel air to the engine face. From the fluid dynamics point of view, a curved duct induces a secondary flow pattern, which essentially sets up "pockets" of swirling flow at the duct exit. Often these pockets of swirling flow occur in pairs and are counterrotating. Also, since our diffuser exit is directly tied into the fan entrance duct, the pockets of swirling flow tend to locally increase or decrease (depending on their direction

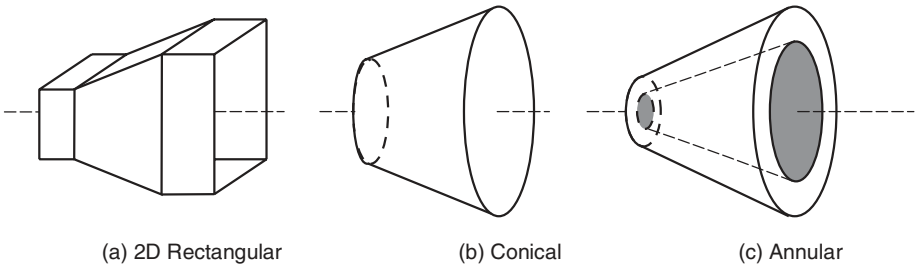

■ **FIGURE 6.4**
Schematic drawing of (subsonic) diffuser geometries with straight centerline

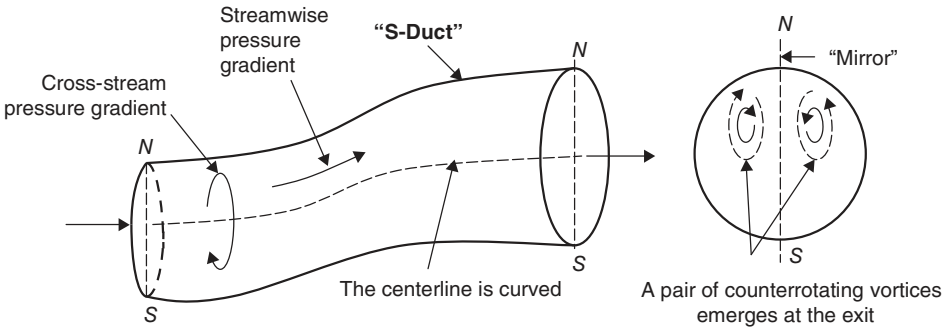

■ **FIGURE 6.5**
Schematic drawing of an S-duct with two pockets of swirling flows (known as the secondary flow pattern) generated by the bends

of rotation) the relative flow angle into the fan, which in turn can lead to cyclic loading of the fan and cause a high-cycle fatigue (HCF) problem. In severe situations, the pockets of swirling flow can produce rotating stall instability of the fan rotor. We will discuss in more detail the compressor/fan inlet flow conditions, that is, the various types of inlet distortion that affect the stability of a compressor flow in the turbomachinery chapter. In Figure 6.5, we show a schematic of a diffuser duct with an S-shaped (curved) centerline.

An aircraft inlet shape may be rectangular for integration and control purposes but it still has to tie in with an engine face, which is circular. Hence, the connecting diffuser duct should continually change its shape from, say, a rectangular to a circular geometry. Such ducts that change their cross-sectional shape are called "transition" ducts and pose interesting fluid mechanic problems due to their highly three-dimensional pressure pattern,

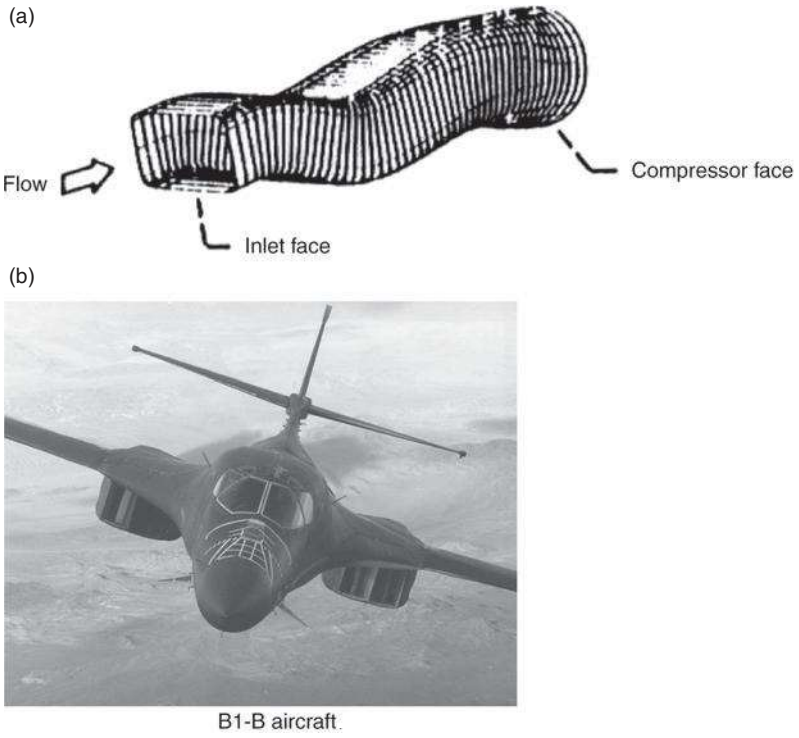

■ **FIGURE 6.6**
Curved-centerline (double-S) transition duct in a B1-B aircraft. Source: (a) Anderson, B.H. 1986. Reproduced with permission from AIAA. (b) Courtesy of USAF

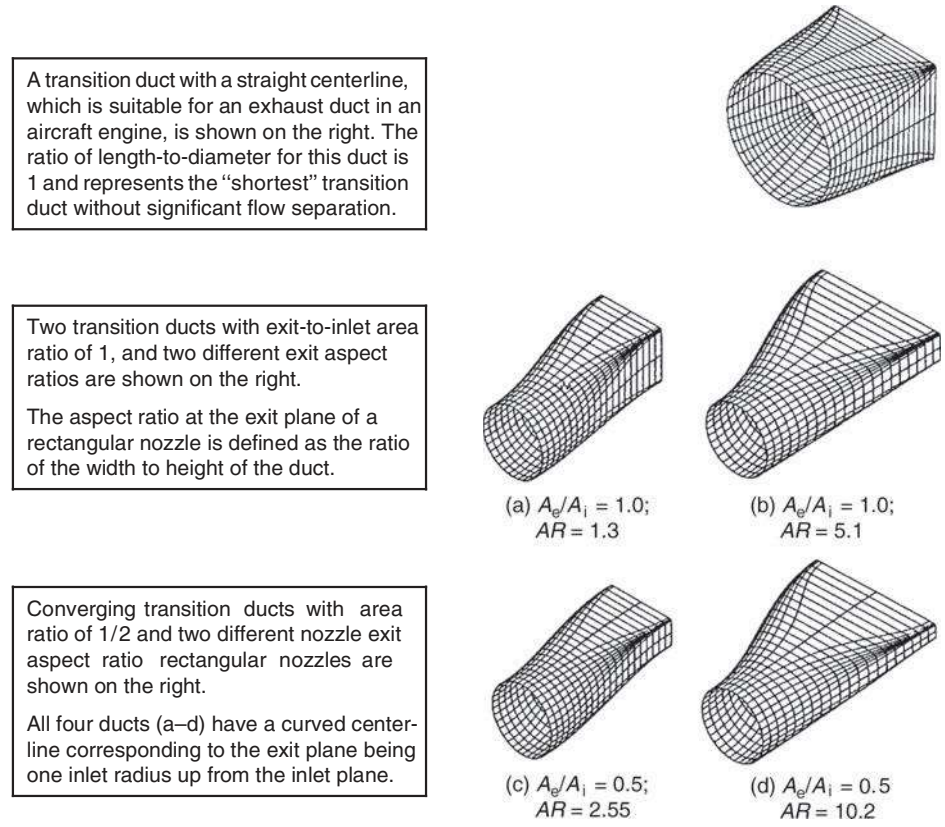

■ **FIGURE 6.7**
Isometric views of various transition ducts with and without centerline curvature. *Note:* that the duct area ratio is shown as A_e/A_i and the duct *aspect ratio* at the exit is shown as *AR*. Source: Farokhi, Sheu, and Wu 1989. Reproduced with permission from Springer

that is, the flowfield. It is interesting to note that the corners in the rectangular portion of a transition duct create, trap, and transport vortices in a complex streamwise and transverse trajectory pattern along the duct's length. Due to their prominence in modern engines, we will examine the viscous flow characteristics in transition ducts more closely in this chapter. The use of transition ducts in an aircraft engine is not limited, however, to the air inlet system. Rather, it includes circular-to-rectangular exhaust systems as well. Rectangular nozzles are useful for stealth, vector thrust, and integration purposes and will be discussed more at the end of this chapter. Figure 6.6 shows the B1-B aircraft inlet transition duct. An isometric view of rectangular nozzle transition ducts with and without curved centerline is also shown in Figure 6.7.

6.6 Subsonic Diffuser Performance

Subsonic diffusers exhibit four different flow regimes, or *stall* characteristics, as presented by Kline (1959) and Kline, Abbot, and Fox (1959). The flow regimes are tied to the quality of exit flow, that is, the state of the boundary layer at the diffuser exit. Although not all different flow regimes are of interest to an aircraft inlet designer, to present the chart and examine various features of the flowfields proves beneficial to all engineers interested in internal fluid mechanics.

- Large capture ratios at takeoff and climb pose a potential problem for engine face distortion
- Wing and aft fuselage-mounted inlets are exposed to flow angularity, that is, droop or toe up angles depending on their placement, that is, the wing upwash or downwash
- Nacelle external contour sets the limitation on high-speed performance of the inlet
- Drag divergence Mach number can be raised by a *supercritical* nacelle design
- Drag reduction may be achieved through a hybrid laminar flow control on the nacelle
- Transition ducts may be needed for integration purposes, sometimes with an offset
- Secondary flow patterns are introduced in ducts with a bend or transition ducts in general, a cause of distortion

There are additional discussions that are relevant to inlets and inlet-aircraft integration:

- Inlet acoustic treatment
- Inlet (cowl) lip icing detection and anti-icing strategies
- Inlet-engine matching, steady-state, and dynamic distortion

Further readings on subsonic inlets and engine installations (references 3, 16, 18, 22, 23, 27, 29, 31, 33, 34, 45 and 47) are recommended.

6.10 Supersonic Inlets

The function of a supersonic inlet is the same as the function of a subsonic inlet, namely, to decelerate the flow to the engine face Mach number requirements (set by the throttle), typically in the range of $M_2 \sim 0.4$–0.6, efficiently, within the entire flight envelope. In practice, flow diffusion from supersonic to subsonic flow involves shocks. Therefore, the study of supersonic inlets is very much dominated by the study of shocks intersecting, interacting, reflecting, and the shock boundary layer interaction. We will also learn that shocks pose instability problems for an inlet and learn possible approaches to stabilizing them. As in subsonic inlets, we are still concerned about the external drag characteristics of the supersonic inlets. Although, there are no supersonic inlet flows that are reversible, we still propose to study them in the limit of reversible, adiabatic flow. By studying isentropic inlets, we learn about throat sizing issues, some off-design Mach numbers, and their impact on the inlet flow behavior.

6.10.1 Isentropic Convergent–Divergent Inlets

By insisting on an isentropic compression, we propose to create an isentropic compression Mach wave system that all converge to a single point, like a fan. It is theoretically possible to machine a concave surface that can decelerate a supersonic flow to a sonic flow. The

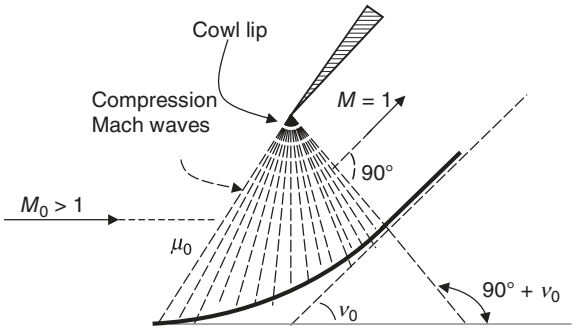

■ **FIGURE 6.25**
An isentropic compression ramp decelerating a supersonic flow to $M = 1$

concave surface is known as an isentropic compression ramp. The picture of the waves set up on an isentropic compression ramp looks like Figure 6.25.

Now let us remember the wave and ramp angles from aerodynamics. We remember that all Mach waves make an angle, called Mach angle, with respect to the *local* flow. Therefore, the lead Mach wave makes an angle

$$\mu_0 = \sin^{-1}(1/M_0) \tag{6.31}$$

The last Mach wave, that is, the tail wave, is normal to the sonic exit flow, that is, $\sin^{-1}(1) = 90°$.We also remember from Prandtl–Meyer flow that the ramp angle of ν_0, which is called Prandtl–Meyer angle, corresponds to turning a *sonic flow* to achieve a supersonic Mach number M_0. Since the process of isentropic compression is reversible, it means that a flow approaching the ramp from the top of Figure 6.25 at sonic speed (i.e., reverse flow) will *accelerate* to achieve M_0 at the bottom of the ramp, the flow turning angle is thus the Prandtl-Meyer angle ν_0 corresponding to M_0. An expression for this angle as a function of Mach number and the ratio of specific heats γ is written as Equation 6.32, which we derived in Chapter 2.

$$\nu(M) \equiv \sqrt{\frac{\gamma+1}{\gamma-1}}\tan^{-1}\sqrt{\frac{\gamma-1}{\gamma+1}(M^2-1)} - \tan^{-1}\sqrt{M^2-1} \tag{6.32}$$

We may decelerate the sonic exit flow from the compression ramp in a subsonic diffuser, which requires a flow area expansion, that is, a diverging duct. Now let us incorporate such isentropic compression ramps in a duct and subsonic diffusers to create a *convergent–divergent* (C–D) duct capable of decelerating a supersonic flow to a subsonic flow reversibly and adiabatically. This duct is then called an isentropic C–D inlet. The simple geometry of it is presented in Figure 6.26.

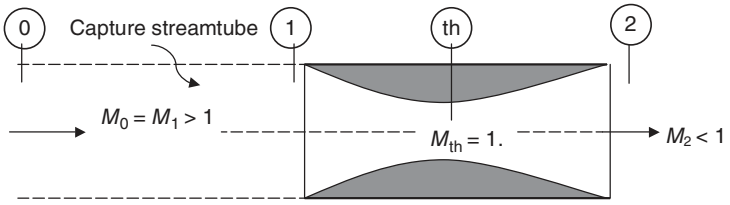

■ **FIGURE 6.26**
Schematic drawing of an isentropic C–D inlet

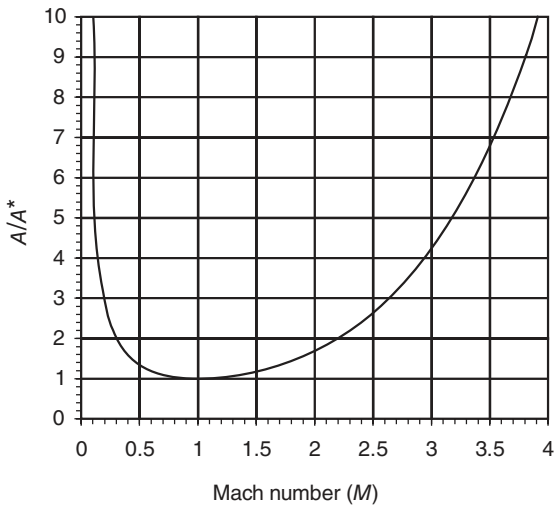

■ **FIGURE 6.27**
Isentropic area ratio as a function of Mach number (γ =1.4) shows that a C–D duct exhibits choking behavior at a supersonic as well as a subsonic Mach number

Let us note that the capture streamtube in Figure 6.26 shows a capture ratio A_0/A_1 of 1, and furthermore its area ratio A_1/A_{th} is uniquely established via an isentropic A/A^* relation corresponding to M_1. For example, the inlet-to-throat area ratio is equal to 2 for an inlet Mach number of 2.2. We can read these numbers from an isentropic table for $\gamma = 1.4$. Also, we note that since the flow deceleration in this inlet takes place entirely within the duct, we may call it an *internal-compression* inlet. The unique isentropic area ratio (A/A^*) at a supersonic speed creates problems at subsonic speeds. Namely, the same area ratio duct *chokes* at a subsonic Mach number too! This means that prior to reaching our target supersonic design Mach number of M_{D}, we have already choked the throat at a subsonic Mach number. Let us return to the example we used in this paragraph. For a supersonic design Mach number of 2.2, the C–D inlet should have its area ratio set at 2.0. By looking up the isentropic tables, in the subsonic portion of it, we note that area ratio 2.0 first chokes at Mach number ~0.3! In other words, each value of A/A^* is repeated twice in the isentropic table, once in the subsonic flow part and then the second time in the supersonic flow portion of the table. Now let us graphically represent the *dual* nature of choking in a compressible flow, that is, (A/A^*) is a *double-valued* function of Mach number. The continuity equation for an isentropic flow established A/A^* according to

$$A/A^* = (1/M)\left[\left(1 + \frac{\gamma - 1}{2}M^2\right) \Big/ \left(\frac{\gamma + 1}{2}\right)\right]^{\frac{\gamma+1}{2(\gamma-1)}} \tag{6.33}$$

We may graph this equation for a range of Mach numbers (Figure 6.27) to demonstrate that there are two Mach numbers, one subsonic and the other supersonic, for each A/A^*.

Now, let us examine the sequence of events that takes place outside and within the inlet from start to the design Mach number. The capture ratio for the inlet starts larger than 1, as in the subsonic inlet at takeoff. The capture ratio remains greater than 1 until the throat chokes at the corresponding subsonic (A/A^*). At this moment, the capture area ratio is 1, and the throat is choked.

Various flow characteristics of an isentropic C–D inlet are shown in Figure 6.28 as a function of flight Mach number. The first choking occurs at a unique subsonic Mach

■ **FIGURE 6.28**
Flow characteristics of an isentropic C–D inlet from low speed to supersonic conditions

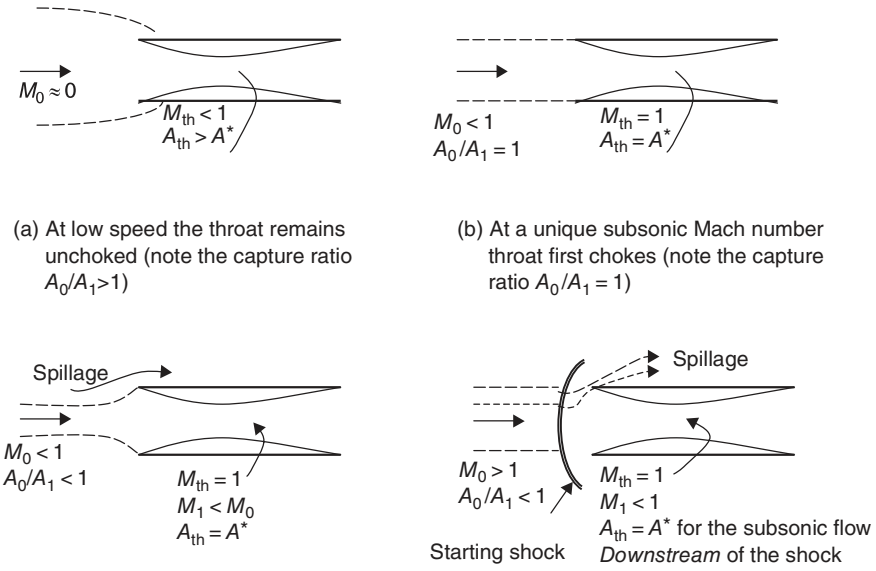

(a) At low speed the throat remains unchoked (note the capture ratio $A_0/A_1 > 1$)

(b) At a unique subsonic Mach number throat first chokes (note the capture ratio $A_0/A_1 = 1$)

(c) At higher subsonic Mach numbers than (b) the capture ratio falls below 1 and spillage occurs (note the throat remains choked)

(d) At supersonic Mach numbers a starting (bow) shock is formed in front of the inlet causing spillage drag while the throat remains choked

number corresponding to the "bucket" graph of (A/A^*) shown in Figure 6.27, where the capture ratio is exactly 1 and no spillage drag occurs. At all Mach numbers above this unique subsonic Mach number, the throat continues to remain choked and the consequence of higher flow manifests itself in a spillage over the inlet lip, as shown in parts (c) and (d) of Figure 6.28. For supersonic flow, a bow shock is formed ahead of the inlet to allow for spillage to occur. The spillage accounts for a choked throat, which is smaller than the corresponding A/A^* at M_0. As long as the starting shock remains in front of the supersonic inlet, the spillage drag and low total pressure recovery are the consequences of this flow. This undesirable condition is called an "unstarted" inlet. We shall now examine a few methods that enable *starting* a C–D inlet.

6.10.2 Methods to Start a Supersonic Convergent–Divergent Inlet

The starting process of a supersonic C–D inlet involves swallowing the starting shock. A normal shock that is brought to the inlet lip is said to be in an incipient starting position. Any disturbance that causes the starting shock to enter the inlet will then result in the shock to move through the convergent portion of the duct and be stabilized at a location in the divergent section downstream of the throat. Normal shocks are therefore said to be unstable in a converging duct. The position of a shock in a duct is dictated by the *backpressure,* which establishes the downstream condition, or outflow condition of the shock. When the backpressure increases, a shock is pushed upstream and when the backpressure decreases, the shock moves downstream. We may use the backpressure principle to explore shock stability in converging as well as diverging ducts. First let us look at a converging duct

that leads to a sonic throat. The starting shock that moves in a converging duct, by virtue of flow area contraction, will experience a decrease in its upstream Mach number M_x. Therefore, the shock *weakens* as it enters a contracting duct. Consequently, the total pressure downstream of the shock in its new position is increased, as the shock is now weaker. The sonic throat, which acts as the first engine throttle, experiences an increased mass flow rate. We remember that the mass flow rate is linearly proportional to the total pressure, that is, $\dot{m} \propto p_t$. The increase in mass flow rate downstream of the shock will reduce the shock backpressure (i.e., it creates a suction), which in turn draws the shock further in the duct and toward the throat. The shock continues moving until it has passed through the throat and is stabilized in the diverging section of the duct. The process of swallowing the starting shock, from the inlet lip to beyond the throat, occurs on the order of convective time scale, namely, $t \sim l/V$, where l is the characteristic diffuser length and V is an average flow speed in the inlet. For a diffuser of ~10 ft or ~3 m length and an average flow speed of ~ 2000 ft/s or ~ 600 m/s, the starting shock should be swallowed on the order of ~ 10/2000 s or ~5 ms. This example shows the abruptness of starting and perhaps most importantly the *unstart* process of a supersonic inlet with an internal throat.

We will address the unstart phenomenon later in this chapter. Now, let us examine the movement of a normal shock downstream of the throat, that is, in the diverging section of a C–D inlet. Assuming the shock is in a position that matches the engine-imposed backpressure condition, any shock motion into the duct will cause M_x to increase, therefore p_t after the shock will drop and the mass flow rate is proportionately reduced. A reduced mass flow rate has the effect of an increased backpressure, which in turn pushes the shock back upstream. So, a displaced shock in the diverging section of a duct returns to its original position, which is the essence of a stable system. A similar argument can be applied to a shock displaced in the opposite direction, that is, closer to the throat. In this case, the upstream Mach number of the shock is reduced, therefore the total pressure downstream of the shock is increased, which causes an increase in the mass flow rate and hence a reduced backpressure, which draws the shock to its original position. Again, we demonstrate shock stability in a diverging duct. We may use Figure 6.29 to graphically depict the starting process.

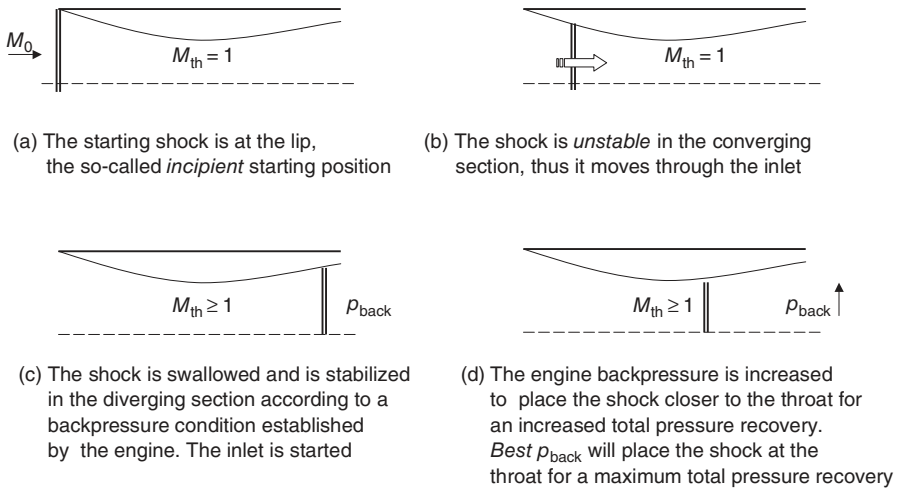

■ **FIGURE 6.29**
Starting sequence of a C–D inlet and the role of backpressure in positioning the shock

(a) The starting shock is at the lip, the so-called *incipient* starting position

(b) The shock is *unstable* in the converging section, thus it moves through the inlet

(c) The shock is swallowed and is stabilized in the diverging section according to a backpressure condition established by the engine. The inlet is started

(d) The engine backpressure is increased to place the shock closer to the throat for an increased total pressure recovery. *Best* p_{back} will place the shock at the throat for a maximum total pressure recovery

■ **FIGURE 6.30**
The starting shock is pushed toward the inlet lip through overspeeding

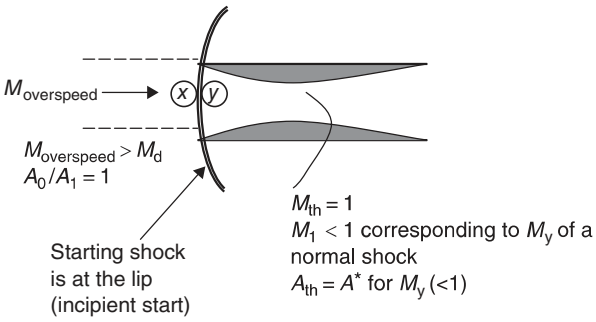

We are now ready to examine different starting methods that will place the starting shock in an *incipient* position, namely, at the inlet lip. These include overspeeding, an enlarged throat, and a variable throat geometry C–D inlet.

6.10.2.1 Overspeeding. For a fixed-geometry C–D inlet, a process of *overspeeding* may start the inlet. This method is feasible for low supersonic design Mach number C–D inlets only. The proposition is to offer a reduced spillage condition on the inlet so as to attract the starting shock toward the inlet lip. Eventually, for an overspeed Mach number $M_{overspeed}$, the starting shock is at the inlet lip. This condition is shown in Figure 6.30 and is known as the incipient inlet start.

EXAMPLE 6.1

Consider an isentropic fixed-geometry C–D inlet, which is designed for $M_D = 1.5$. Calculate the overspeed Mach number that will start this inlet.

SOLUTION

We first establish the design area ratio A_1/A^{th} for a design Mach number of 1.5. From the isentropic table for $\gamma = 1.4$, we have

$$A_1/A_{th} = A_1/A^* = 1.176$$

Now, if the starting shock is at the lip, the subsonic flow at M_y will have the same A/A^* as the inlet, since the throat is still choked. Therefore we look up the isentropic table for a subsonic Mach number, which corresponds to this area ratio

$$A_y/A^* = 1.176 \xrightarrow[M<1]{\text{Isentropic table}} M_y \approx 0.61$$

From a normal shock table, we establish a corresponding upstream Mach number M_x or $M_{overspeed}$.

$$M_y \approx 0.61 \xrightarrow{\text{Normal shock table}} M_x \approx 1.80$$

Therefore,

$$\boxed{M_{overspeed} \approx 1.80}$$

Now, let us examine an aerodynamic limitation of overspeeding. For this purpose, we assume an infinite overspeed is possible (although both structurally and propulsively impossible). From the normal shock (NS) table, we have

$$M_x \sim \infty \text{ yields a } M_y \to \sim 0.378$$

Now we look up the isentropic area ratio A/A^* corresponding to $M_y = 0.378$.

$$M_y \approx 0.378 \xrightarrow{\text{Isentropictable}} A_y/A^* \approx 1.666 = A_1/A_{th}$$

For this area ratio, we find a corresponding supersonic Mach number, which then represents the design Mach number M_D

$$A_1/A^* \approx 1.666 \xrightarrow[M>1]{\text{Isentropictable}} M_1 = M_D \approx 1.99$$

(requires infinite overspeeding)

This example shows that through overspeeding, we cannot even start a C–D inlet designed for a design Mach number of $M_D = 2$. We alluded to structural limitations, infinite loads, as well as propulsive limitations, that is infinite thrust, earlier which prevent infinite overspeeding as a means of starting an inlet. With these limitations, we examine an enlarged throat C–D inlet that is capable of self-starting at the design Mach number. This is called Kantrowitz–Donaldson inlet.

6.10.2.2 Kantrowitz–Donaldson Inlet. Consider a C–D inlet with an enlarged throat area that eliminates spillage of an isentropic C–D inlet at design Mach number. Therefore, we are interested in a C–D duct with a unique contraction ratio that places the starting shock at the inlet lip at the design Mach number. This is called a Kantrowitz–Donaldson (K–D) inlet, which has a self-starting capability (Kantrowitz and Donaldson, 1945). By virtue of having absorbed the spillage mass flow rate at the design Mach number, the throat area of a K–D inlet has to be larger than that of the corresponding isentropic inlet. Let us graph this proposition (Figure 6.31).

We may quantify the K–D inlet contraction ratio since from the design Mach number, we can establish M_y, which is the M_1 just downstream of the shock. Also assuming an isentropic flow downstream of the shock, we may establish the required area ratio A_1/A_{th}. Once the shock is swallowed and stabilized downstream of the throat, the throat Mach number will be greater than 1. The best backpressure will place the shock at the throat. Note that a normal shock at the throat is unstable and could lead to the phenomenon of unstart, or the shock sweeping backwards through the inlet and causing tremendous spillage drag as well as a loss of engine thrust. For this reason, all supersonic inlets with an internal throat need to actively control the position of the terminal shock in the diverging section of the duct. We will address this issue later in this chapter. Let us graphically depict the various phases of a K–D inlet flow environment from design Mach number M_D to the best backpressure (Figure 6.32a).

We now solve a problem that demonstrates the geometry and capabilities of a K–D inlet.

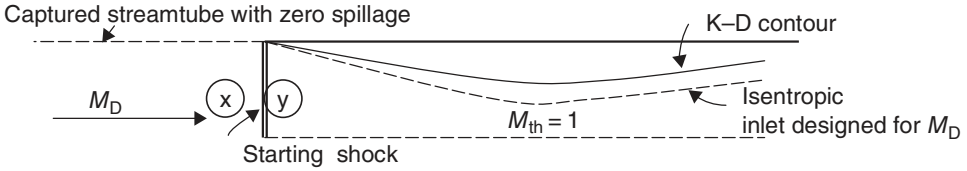

■ **FIGURE 6.31 A K–D inlet at design Mach number (at the moment of incipient start); also note the larger throat area of a K–D inlet as compared with an isentropic inlet designed for M_D**

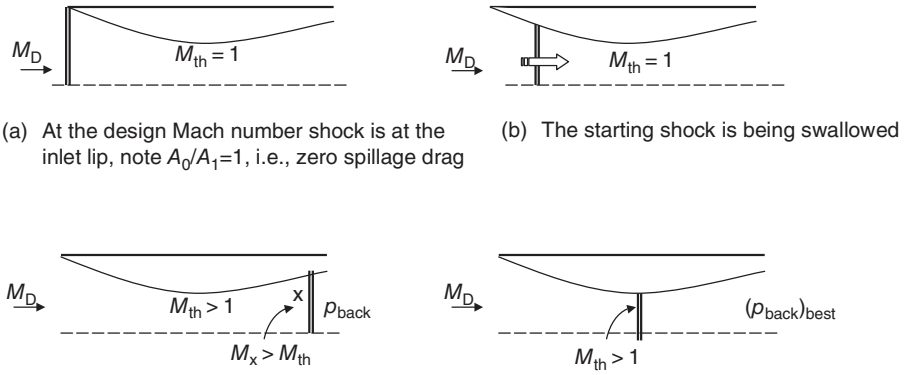

■ **FIGURE 6.32** **The sequence of events in a Kantrowitz–Donaldson inlet**

(a) At the design Mach number shock is at the inlet lip, note A_0/A_1=1, i.e., zero spillage drag

(b) The starting shock is being swallowed

(c) Shock is in a stable position, the throat is unchoked ($M_{th} > 1$)

(d) The best backpressure places the shock at the throat

EXAMPLE 6.2

Calculate the contraction ratio A_1/A_{th}, and the maximum total pressure recovery of a self-starting C–D inlet designed for $M_D = 2.65$.

SOLUTION

At the design Mach number, a self-starting inlet has its starting shock at the lip (Figure 6.32a), therefore

$$M_D = M_x = 2.65 \xrightarrow{\text{Normal shock table}} M_y = 0.4996 = M_1$$

$$M_1 = 0.4996\ (\sim 0.5) \xrightarrow{\text{Isentropic table}} A_1/A^*$$

$$\equiv 1.34 = A_1/A_{th}$$

$$\therefore \quad \boxed{A_1/A_{th} \equiv 1.34}$$

The best backpressure places the shock at the throat, thus we need to calculate the throat Mach number M_{th} after the inlet was started. From Figure 6.32c, we note that a supersonic flow at the design Mach number enters the inlet and assuming isentropic deceleration to the throat, we may arrive at the throat Mach number, via the following steps

$$M_D = 2.65 \xrightarrow{\text{Isentropic table}} A_1/A^* = 3.036$$

$$A_{th}/A^* = (A_1/A^*)/(A_1/A_{th}) = 3.036/1.34$$
$$= 2.2656 \xrightarrow{\text{Isentropic table } M>1} M_{th} \sim 2.35$$

Now we need to place a shock at this Mach number, i.e.

$$(p_{ty}/p_{tx})_{\text{best backpressure}} \xrightarrow{\text{Normal shock table } M_x \sim 2.35}$$

$$\boxed{p_{ty}/p_{tx} \sim 0.5615}$$

Note that the price of a fixed-geometry self-starting C–D inlet is a high throat Mach number and subsequent large total pressure loss. We calculated the throat Mach number, i.e., the lowest Mach number in the duct, of a started K–D inlet designed for Mach 2.65 is ~2.35. This performance penalty of a fixed-geometry inlet suggests the potential advantage of a variable geometry throat inlet. We shall examine such inlets next.

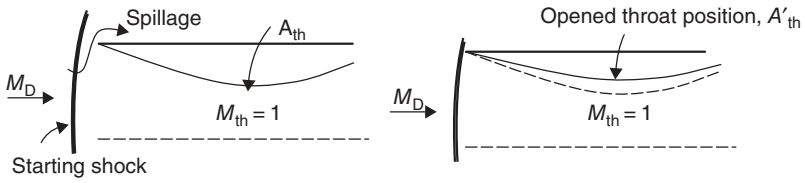

■ **FIGURE 6.33** Variable-geometry C–D inlet starts by enlarging its throat area (from A_{th} to A'_{th})

(a) Starting shock with spillage at M_D

(b) Incipient start position is achieved by opening the throat to absorb spillage flow

6.10.2.3 Variable-Throat Isentropic C–D Inlet. To eliminate spillage flow and attract the starting shock to the inlet lip, a variable geometry inlet opens up its throat to accommodate a higher flow rate and thus begin the starting process. The two shock positions prior to the starting and at the incipient start condition are shown in Figure 6.33.

After the starting shock has swept through the opened throat in the starting process, the throat Mach number becomes supersonic. The opening size of the throat and the throat Mach number are identical to those of the Kantrowitz–Donaldson inlet. However, in this case of variable geometry, we can proceed to close the inlet throat back to its original sonic condition/dimension. The attractiveness of this method of starting a supersonic inlet with an internal throat is the potential for high total pressure recovery, that is, high performance. The price for this performance is paid through the added system weight and complexity associated with multisegmented inlet with actuators, sensors, and a controller needed to operate the inlet.

Now, let us learn, through a sample problem, the important parameters associated with a variable-geometry inlet, namely, the percantage opening of the throat needed to start the inlet, the throat Mach number after the inlet has started.

EXAMPLE 6.3

A supersonic convergent–divergent inlet is to be designed for an isentropic operation (in the started mode) at $M_D = 3.3$. Calculate the inlet design contraction ratio A_1/A_{th}, the percantage opening of the throat $(A'_{th} - A_{th})/A_{th}$ needed to start the inlet, and the throat Mach number in the open position M'_{th}.

SOLUTION

First, the isentropic area ratio for M_D is read from the isentropic table to be

$$M_D = 3.3 \xrightarrow{\text{Isentropic table}} A_1/A^* = A_1/A_{th} = 5.629$$

Now, at the opened throat position, the starting shock is at the lip, therefore,

$$M_D = M_x = 3.3 \xrightarrow{\text{Normal shock}} M_y = M_1$$
$$= 0.4596 \xrightarrow{\text{Isentropic table}} A_1/A'_{th} \equiv 1.425$$

Now, we can calculate the percantage throat opening according to

$$\frac{A'_{th} - A_{th}}{A_{th}} \times 100 = \left(\frac{\frac{A'_{th}}{A_1} - \frac{A_{th}}{A_1}}{\frac{A_{th}}{A_1}} \right) \times 100$$
$$= \frac{(1/1.425) - (1/5.629)}{1/5.629} \cong 295\%$$

Our calculations indicate that the opened throat is roughly three times the size of the isentropic throat to start the inlet designed for Mach 3.3. We can calculate the flow Mach number at the throat, in the open position, once the shock is stabilized downstream of the throat. To get the Mach number we need A'_{th}/A^*, similar to the K–D inlet calculation, namely,

$$A'_{th}/A^* = (A'_{th}/A_1)/(A^*/A_1) = (1/1.425)/(1/5.629)$$
$$\cong 3.950 \xrightarrow{\text{Isentropic table } M>1} M'_{th} \sim 2.95$$

We finally proceed to close the throat to achieve $M_{th} = 1$ and a near isentropic flow condition.

6.11 Normal Shock Inlets

A sharp-lipped subsonic diffuser may be used in a supersonic stream without a significant aerodynamic penalty if the free stream Mach number is below ~ 1.6. As for all supersonic inlets, a shock is formed at or near the inlet, which decelerates the supersonic flow to subsonic. The sharp lip geometry allows for an attached shock, whereas a blunt cowl leading edge creates a bow shock with the attendant external drag penalty. This type of supersonic inlet is short, light weight, and with no movable surfaces, which is suitable for low supersonic Mach applications or low-cost weapon systems development. Let us define the geometry and salient features of a normal shock inlet in Figure 6.34.

The position of the normal shock depends on the inlet backpressure, which is established by the engine. The best backpressure, corresponding to design Mach number, places the normal shock at the lip where the best total pressure recovery coincides with zero spillage drag. This mode of operation is called the *critical* mode. In the event of higher backpressure, that is, when the engine mass flow rate drops, the shock stands outside the inlet and a spillage flow takes place. This is the so-called *subcritical* mode of operation. The shock is drawn into the inlet, beyond the lip, when the engine backpressure is lowered. This is the so-called *supercritical* mode of operation. In the supercritical mode, the shock Mach number is higher than M_0, hence a larger total pressure drop in the inlet results. Consequently, the corrected mass flow rate at the engine face increases, which results in an increase in axial Mach number, thereby, reducing the engine face static pressure, that is, the inlet backpressure. Furthermore, the shock inside the duct may interact adversely with the wall boundary layer and cause separation and increase engine face distortion.

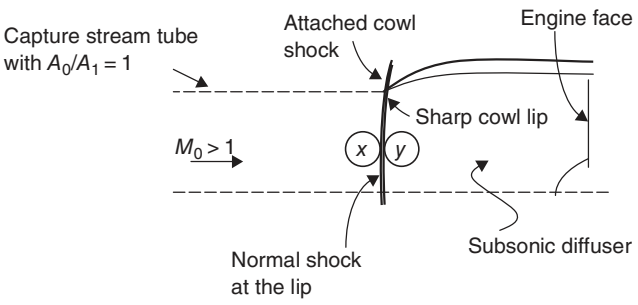

■ **FIGURE 6.34**
Normal shock inlet is shown with the shock at the lip

■ **FIGURE 6.35**
Three modes of operation of a normal shock inlet show the subcritical mode as an external-performance limiting and the supercritical mode as the internal performance limiting flow conditions with the best mode identified as the critical mode

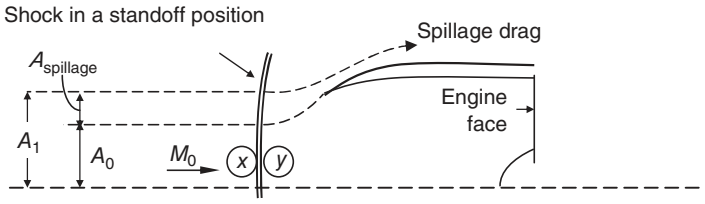

(a) Normal shock inlet in *subcritical mode* (*high* backpressure–low m and m_{cor})

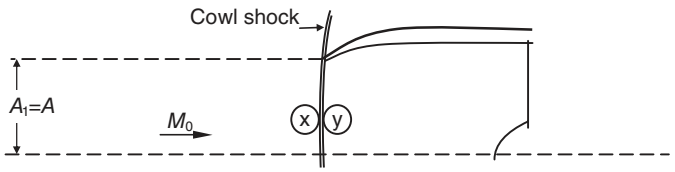

(b) Normal shock inlet in *critical mode* (*low* backpressure–$\dot{m}_{Design}$)

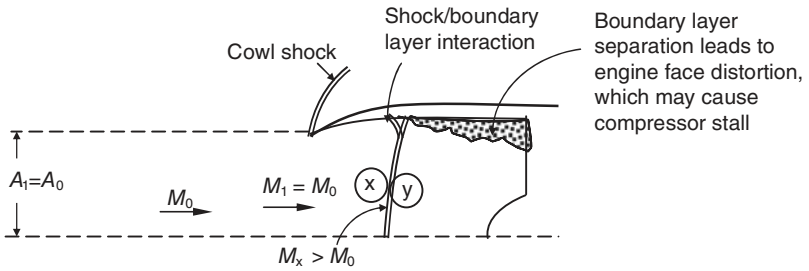

(c) Normal shock inlet in *subcritical mode* (*low* backpressure–higher $\dot{m}_{cor,}$ and $\dot{m}_{Design}$)

Note that a normal shock inlet has its throat at the lip and hence experiences no starting problem. Even in the sub or supercritical modes the shock is stable. The three modes of operation of a normal shock inlet are shown in Figure 6.35. It is also customary to present the off-design performance of supersonic inlets as a plot of their total pressure recovery versus the inlet mass flow ratio. The design mass flow rate is used as the reference value to create a dimensionless mass flow ratio. A typical graph of shock total pressure recovery versus the mass flow ratio for a NS-inlet is shown in Figure 6.36.

■ **FIGURE 6.36**
Typical performance plot of a normal shock inlet

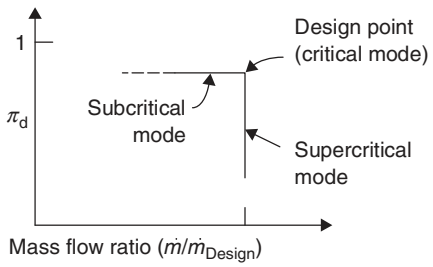

■ **FIGURE 6.37**
Normal shock recovery as a function of Mach number ($\gamma = 1.4$)

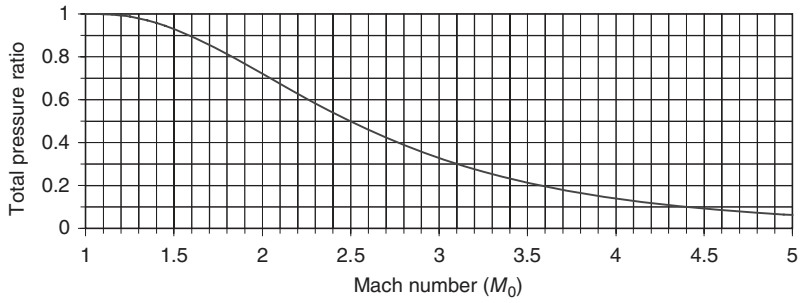

The total pressure recovery of a normal shock rapidly deteriorates beyond Mach ~ 1.6, where a ~90% total pressure recovery is achieved. The normal shock recovery as a function of Mach number is graphed in Figure 6.37.

EXAMPLE 6.4

A normal shock inlet operates in a Mach 1.4 stream. Calculate

(a) inlet total pressure recovery with the shock at the lip, i.e., the best backpressure

(b) inlet total pressure recovery when the shock is inside the duct at $A_x/A_1 = 1.1$, i.e., the supercritical mode

(c) inlet total pressure recovery in subcritical mode with 10% spillage, i.e., $A_{\text{spillage}}/A_1 = 0.1$

SOLUTION

We need to establish the shock Mach number in each mode of inlet operation. In case (a), where the shock is at the lip, representing the best backpressure, the shock Mach number is M_0, therefore,

$$M_0 = 1.4 \xrightarrow{\text{Normal shock table}} \boxed{p_{t2}/p_{t0} = 0.9582}$$

To calculate the shock Mach number when the shock is inside the inlet, we note that the inlet flow may be assumed isentropic all the way to the shock. Hence, we will use A/A^* at the shock, based on upstream flow, to establish the shock Mach number M_x.

$$A_x/A^* = (A_x/A_1)(A_1/A^*)$$

The position of the shock inside the inlet is given as $A_x/A_1 = 1.1$ in the problem statement. The ratio A_1/A^* is purely a function of M_1 via isentropic flow relations, which is known to be $M_1 = M_0 = 1.4$. Therefore,

$$M_1 = 1.4 \xrightarrow{\text{Isentropic table}} A_1/A^* = 1.115$$

$$A_x/A^* = (1.1)(1.115) = 1.226 \xrightarrow{\text{Isentropic table } M>1}$$

$$M_x \approx 1.56 \xrightarrow{\text{Normal shock table}} \boxed{p_{t2}/p_{t0} \approx 0.91}$$

Note that the shock Mach number M_x is higher than M_0 as expected (supersonic Mach number goes up in a diverging duct, i.e., with flow area increase). Also, note that the total pressure recovery is reduced in case (b), again as expected. The other penalty of the supercritical mode of operation is the potential boundary layer separation and engine face distortion, which are complex fluid phenomena and beyond the scope of the present text.

Now, let us address the case (c), where the shock stands outside the inlet and causes spillage. It is quantified as causing a 10% spillage, which is $1 - A_0/A_1$. The shock Mach number, however, is the same as M_0, hence the same total pressure recovery is expected, i.e.,

Since $M_x = M_0$ in subcritical mode, then

$$\boxed{p_{t2}/p_{t0} = 0.9582}$$

However, we note that the penalty for subcritical mode of operation is the spillage drag D_{spillage}.

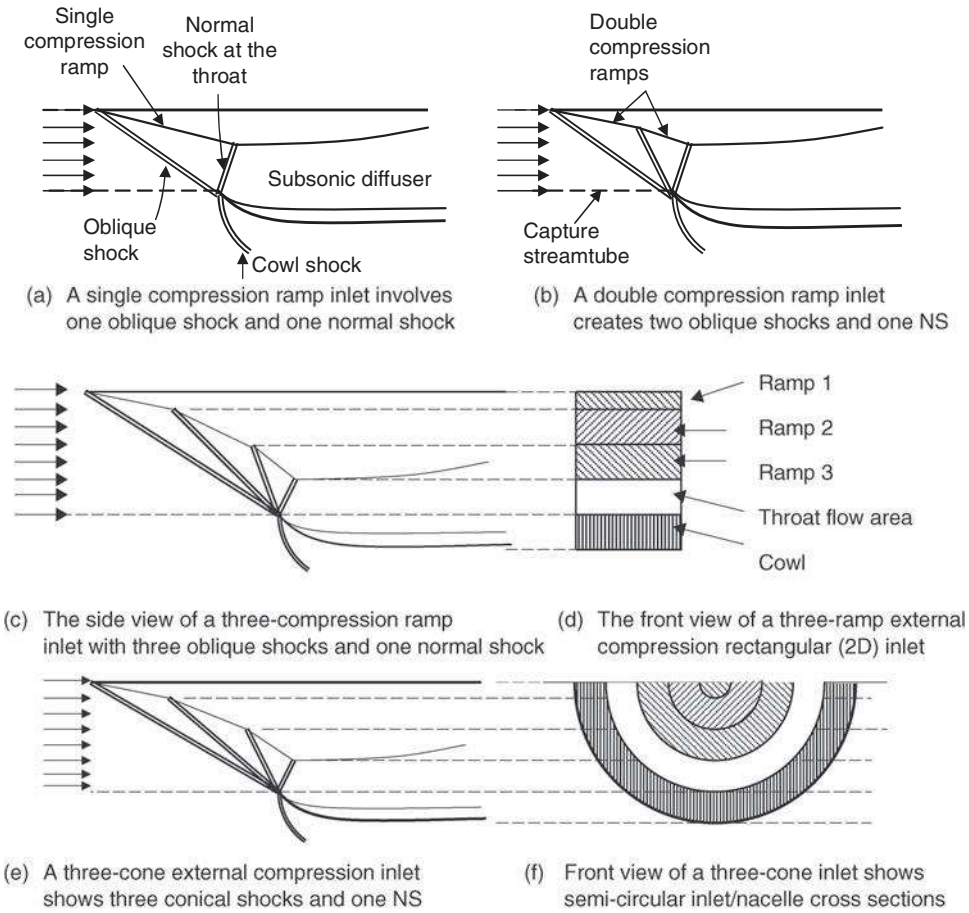

■ **FIGURE 6.38** **Shock systems of two-dimensional and axisymmetric external compression inlets with the best backpressure placing the terminal (normal) shock at the lip (throat)**

6.12 External Compression Inlets

To achieve a higher total pressure recovery than a normal shock inlet, we need to design an inlet configuration that incorporates multiple shocks. Supersonic flow deceleration over multiple shocks is more efficient than the deceleration through a normal shock. Here, the efficiency of the supersonic diffusion process is defined by the total pressure recovery of the shock system. An external compression inlet is designed to maintain the shock system external to the inlet and, hence, has its throat at the cowl lip. The internal duct is hence a subsonic diffuser, which is often a transition duct with offset. Two-dimensional external compression inlets employ external compression ramps to create plane oblique shocks, whereas axisym-metric inlets employ multiple cones to create conical shocks. Single and multiple ramp external compression inlets as well as axisymmetric inlets are shown in Figure 6.38. The position of the normal shock, which is also called a *terminal shock,* is dictated by the inlet backpressure. The optimal location for the normal shock is at the throat where the flow Mach number is the least. With the normal shock at the cowl lip,

the inlet is said to operate at its critical mode, which represents the design point. Figure 6.38 shows several external compression inlets at their design point operation.

The total pressure recovery of the inlet shock system may be calculated via a straightforward marching technique that we learned in supersonic aerodynamics. Assuming the geometry of the external compression ramp is known (the so-called *design problem),* each ramp angle represents the flow turning θ, which combined with the information on the local Mach number M, leads to a determination of the wave angle β, by using a θ-β-M oblique shock chart (or conical shock charts). The wave angle helps establish the strength of the oblique shock, which depends on the normal component of the flow to the shock, namely, $M_n = M \sin\beta$. Since the local Mach number is only a priori known in station 0, that is, the free stream condition, we need to start with the first oblique shock and continue marching downstream through multiple ramps and shocks. This method is best illustrated through an example.

EXAMPLE 6.5

A two-ramp external compression inlet in a supersonic flow is shown. Calculate the total pressure recovery of this inlet assuming the best backpressure has placed the normal shock on the lip. Also compare this inlet to a NS-inlet at Mach 2.0

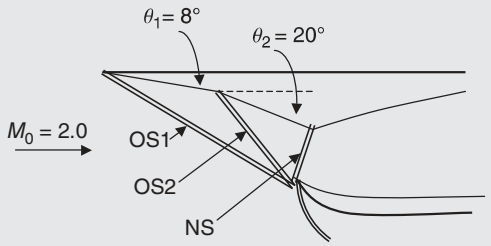

SOLUTION

The shock total pressure recovery as a function of Mach number M and the wave angle β is

$$\frac{p_{t2}}{p_{t1}} = \frac{\left(\dfrac{\frac{\gamma+1}{2}M^2\sin^2\beta}{1+\frac{\gamma-1}{2}M^2\sin^2\beta}\right)^{\frac{\gamma}{\gamma-1}}}{\left(\dfrac{2}{\gamma+1}M^2\sin^2\beta - \dfrac{\gamma-1}{\gamma+1}\right)^{\frac{1}{\gamma-1}}}$$

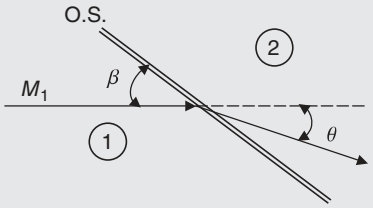

Therefore, we need to establish the wave angles and the local Mach numbers upstream of every shock. Using an oblique shock chart $\theta-\beta-M$, any pair of values determines the third. For the first oblique shock (OS1) we know the Mach number and the flow turning angle, i.e.,

OBLIQUE SHOCK 1

$$\left.\begin{matrix} M_0 = 2.0 \\ \theta = 8° \end{matrix}\right\} \xrightarrow{\theta-\beta-M \text{ chart}} \boxed{\beta_1 \approx 37°} \Rightarrow M_{n1} = M_0 \sin\beta = 2\sin 37° \equiv 1.20 \Rightarrow (p_{t2}/p_{t1})_{OS1} \cong 0.993$$

Also, from a normal shock table (or the following equation), we get M_n downstream of the first shock, i.e.,

$$M_{n2}^2 = \frac{2 + (\gamma - 1)M_{n1}^2}{2\gamma M_{n1}^2 - (\gamma - 1)}$$

$$M_{n1} \cong 1.2 \Rightarrow M_{n2} = 0.843 \Rightarrow M_2 = M_{n2} / \sin(\beta - \theta) \cong 0.843 / \sin 29^\circ \cong 1.74$$

Now, we are ready for the oblique shock 2.

OBLIQUE SHOCK 2 We need the Mach number, which was calculated from above to be 1.74 and the turning angle through the second shock. Although the ramp angle is shown to be 20°, note that the flow had already turned by 8° through the first oblique shock, therefore the net turning angle through the second shock is only 12°, hence

$M \cong 1.74$, $\theta = 12^\circ$ → Oblique shock chart → $\boxed{\beta_2 \approx 48{:}7^\circ}$ $\Rightarrow M_{n1} = 1.74 \sin 48.7^\circ \equiv 1.31 \Rightarrow (p_{t2}/p_{t1})_{OS2} \cong 0.978$

$$M_{n1} = 1.31 \Rightarrow M_{n2} \cong 0.782$$

$$M_2 = \frac{M_{n2}}{\sin(\beta - \theta)} \Rightarrow M_2 \cong 0.782 / \sin(36.7^\circ) \cong 1.31$$

NORMAL SHOCK We calculated the local Mach number downstream of the OS2 as $M = 1.31$. Since the flow is normal to the terminal shock, $\beta = 90^\circ$, which may be substituted in the above equation for p_{t2}/p_{t1} or simply use a normal shock table.

$$M \cong 1.31,\ \beta = 90^\circ \Rightarrow (p_{t2}/p_{t1})_{NS} \cong 0.977$$

Overall shock total pressure recovery

$$(p_{t2}/p_{t1})_{overall} \cong (p_{t2}/p_{t1})_{OSI}\,(p_{t2}/p_{t1})_{OSI2}\,(p_{t2}/p_{t1})_{NS} \cong (0.993)(0.978)(0.977) \equiv 0.949$$

$$\boxed{p_{t2}/p_{t1})_{overall} \cong 0.949}$$

COMPARISON TO A NORMAL SHOCK INLET A normal shock inlet at Mach 2, with the best back-pressure gives a dismal performance, i.e.,

$$\boxed{(p_{t2}/p_{t1})_{NS} \cong 0.721}$$

We see a tremendous improvement in total pressure recovery where multiple ramps are used.

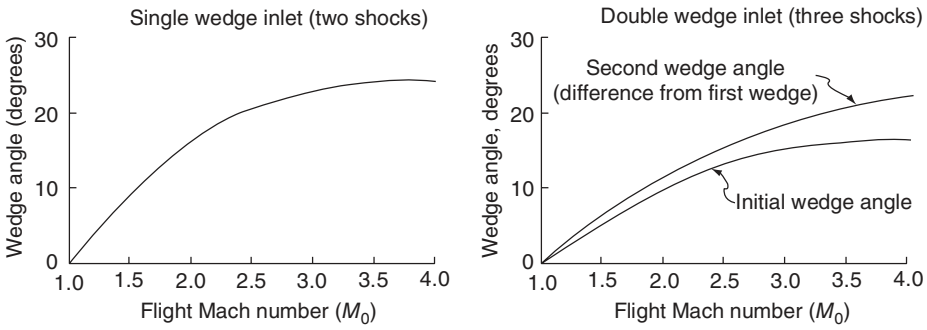

■ **FIGURE 6.39**
Optimum ramp angles for a single and double-ramp external compression inlet. Source: Rodean 1958

6.12.1 Optimum Ramp Angles

In the previous problem, we arbitrarily chose two ramp angles of 8° and 12° net turning, respectively, for our Mach 2.0 inlet. This design recovered nearly 95% of total pressure through the shock system. A question of optimization arises as to the optimum ramp angles, which lead to a maximum pressure recovery at a given Mach number. So, let us restate the problem in general terms as follows:

Find optimum ramp angles for a multiramp external compression inlet designed for $M_0 > 0$.

This fundamental aerodynamic question was raised and answered by Oswatitsch in a 1944 German report (translated into English in 1947 as a NACA report). The result is astonishingly simple. It states that in an optimum multishock inlet, all shocks need to be of equal strength. This speaks to the *principle of equal burden.* Hesse and Mumford (1964) in their classical propulsion textbook produced the optimum geometries for a single and double ramp external compression inlet. These are shown in Figures 6.39 and 6.40.

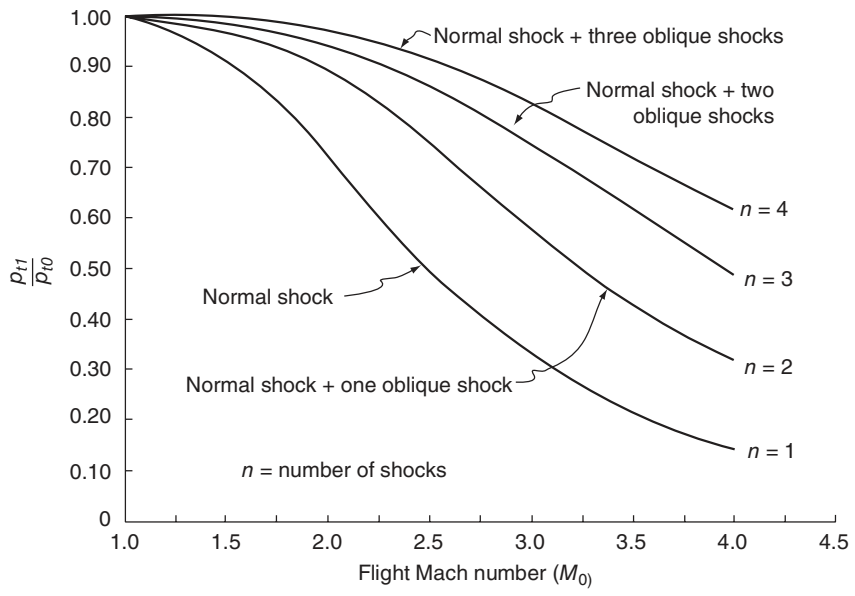

■ **FIGURE 6.40**
Optimum total pressure recovery of external compression inlets. Source: Rodean 1958